small methods
www.small-methods.com

Intelligent Multifunctional Sensing Systems based on Ordered Macro-Microporous Metal Organic Framework and Its Derivatives

Jing Wang, Yuan Ren, Wei Li, Limin Wu, Yonghui Deng,* and Xiaosheng Fang**

Compared with nanomaterials-based sensors with single function, the development of multifunctional sensors shows high potential in comprehensive monitoring of personal health and environment, intelligent human-machine interfaces, and realistic imitation of human skin in prosthetics. Ordered macro-microporous metal-organic frameworks (MOFs)-enabled flexible and stretchable electronics are promising candidates for integrated multifunctional sensing systems. Herein, a three-dimensional ordered macro-microporous zeolite imidazolate framework-8 (3DOM ZIF-8) for humidity sensing and the derived ZnO within a hierarchically ordered macroporous-mesoporous-microporous carbon matrix (ZnO@HOMC) for gas sensor is constructed. Benefit from hierarchically ordered macroporous-mesoporous-microporous structure, the active site is fully exposed, and the charge transfer is accelerated. As a result, the multifunctional sensing systems show ultrafast response and recovery speed (10 s and 34 s), high sensitivity (R_{air}/R_{gas} = 38.6@50 ppm) to acetone, rapid humidity response speed (0.23 s) within changing humidity (RH 21%–99%), excellent stability and repeatability. Furthermore, in order to realize real-time monitoring of gas concentrations and humidity on mobile devices, an intelligent and portable sensor module is fabricated and wirelessly connected to a smartphone to effectively detect acetone concentration and humidity. This sensing technology shows fascinating applications in personal health, fitness tracking, electronic skins, artificial nervous systems, and human-machine interactions.

1. Introduction

Due to the exceptional tunability of structures,[1] MOFs with highly porous structures have been systematically exploited for applications of gas or humidity detection.[2,3] The porous structure of MOFs can effectively concentrate the analyte molecules at high levels.[4,5] The sensitivity, selectivity, response speed, long-term stability, and reusability are important parameters to evaluate the multifunctional sensing performances of MOFs.[6,7] Despite the impressive achievements of sensing performance based on MOFs, multifunctional detection of various stimuli still remains huge challenge to expand its practical applications.[8] The adsorption capacity of MOFs to signal molecules depends on their pore size and aperture size,[9] which are the key to produce improved sensing performances.[10] Topological features particularly pore sizes at each dimension and uniformity are key factors to maintain overall crystalline order, which can afford significantly improved sensing properties.[11] A few advantageous examples include substantially improved conductivities and electron mobilities

J. Wang, W. Li, L. Wu, X. Fang
Department of Materials Science
State Key Laboratory of Molecular Engineering of Polymers
Institute of Brain Intelligence Science and Technology
Fudan University
Shanghai 200433, P. R. China
E-mail: lmw@fudan.edu.cn; xshfang@fudan.edu.cn

Y. Ren, Y. Deng
Department of Chemistry
State Key Laboratory of Molecular Engineering of Polymers
Shanghai Key Laboratory of Molecular Catalysis and Innovative Materials
Fudan University
Shanghai 200433, P. R. China
E-mail: yhdeng@fudan.edu.cn

Y. Ren
School of Materials Science and Engineering and Jiangsu Key Laboratory for Advanced Metallic Materials
Southeast University
Nanjing 211189, P. R. China

L. Wu
College of Chemistry and Chemical Engineering
Inner Mongolia University
Hohhot 010021, P. R. China

The ORCID identification number(s) for the author(s) of this article can be found under https://doi.org/10.1002/smtd.202201687

DOI: 10.1002/smtd.202201687

for much stronger framework acidities and stabilities for mesoporous crystalline zeolites imidazolate with respect to amorphous molecular sieves.[12,13] The single crystal with a three-dimensional ordered macro-microporous structure shows improved mass diffusion properties and robust single-crystalline nature,[11] which is promising candidate for constructing sensing devices.[12] Their superior catalytic activity and recyclability for molecule reactions make it outperform the conventional MOFs and disordered macroporous ZIF-8.[13]

Intelligent sensors based on the three-dimensional ordered macro-microporous metal-organic frameworks (MOFs) would be one of the most effective strategy for continuous monitoring of physiological and environmental indicators,[2] including harmful gas concentration,[3] humidity level,[14] and temperature,[15] offers valuable information for the prediction and management.[13] Although the state-of-the-art developed intelligent devices show superior performance,[16] they are usually limited to a single function to the target and can only work under specific conditions,[7] which cannot meet the requirements of miniaturization, multifunction, and flexibility.[17] In this context, intelligent multifunctional sensing devices have been deeply concerned by industry and academia due to their several advantages,[18] such as high sensitivity, low power consumption, and low cost.[19–21] To achieve these characteristics, three-dimensional ordered macro-microporous metal-organic frameworks (3DOM MOFs) together with its derivatives,[22] potentially in less resistance to mass transfer and compatibility with low-cost manufacturing process, can also realize simultaneous multistimulus sensing and achieve a large-area expandability and adjustable sensing range.[23] Although there have been some reports about MOFs and their derivatives for humidity and gas sensing, they rely on a few kinds of electron-conductive MOFs and were limited to single function.

As a kind of volatile organic compounds, acetone can easily enter the lungs as the by-product of human breathing metabolism, leading to affected by a variety of diseases.[24] Long-term exposure to acetone at low concentration will cause dizziness, muscle weakness, fatigue, and kidney damage.[25] The humidity environment is also critical for supporting human activities, and appropriate humidity can avoid illnesses and discomforts that lead to the change of respiratory frequency and depth, such as heart disease, pneumonia, bronchitis, and sleep apnea syndrome.[26] Therefore, humidity and respiratory gas analysis makes sense for clinical applications.[27] It is desperate to develop intelligent multifunctional sensor such as humidity and gas sensing system for industrial environment monitoring and human health. However, novel nanomaterials with high-performance, flexible and stretchable structures are highly scarce for practical applications in manufacturing of multifunctional sensing devices. In this regard, the integration of simultaneous multistimulus sensing and 3D-ordered macroporous structure to further improve their sensing performance is highly demanded but has never been realized.

Herein, we proposed a sensor integrated with multifunctional sensing system based on three-dimensional ordered macro-microporous zeolite imidazolate framework-8 (3DOM ZIF-8) and its derivatives (ZnO@HOMC). This sensing system can respond to both gas and humidity stimuli under outdoor conditions for development of next-generation intelligent systems. In addition, the multifunctional sensor shows high linearity, high resolution without time delay. Our work represents a good example to integrate a sensing system to achieve highly specific and sensitive detection, which could meet the requirements of wearable electronic for real-time monitoring of environmental conditions under different stimuli.[7] We further construct a personalized intelligent prosthesis and use it in real-time spatial gas content and humidity estimation.[28] Looking forward, this multifunctional sensor has broader applications in health monitoring, humanoid robotics, prosthetics, and human-machine interfaces.

2. Results and Discussion

The preparation procedure of 3DOM ZIF-8 is shown in **Figure 1**. First, ordered 3D monoliths assembled by monodisperse polystyrene(PS) spheres were soaked in a methanol solution containing $Zn(NO_3)_2{\cdot}6H_2O$ and 2-methylimidazole followed by ZIF-8 crystallization to form ZIF-8@PS through the addition of mixed ammonia-methanol solution.[18] After removing PS templates by dimethylformamide and dichloromethane treatment, the 3DOM ZIF-8 was obtained.[4] The obtained hierarchically interconnected structure consists of two kinds of pores. The micropores were from ZIF-8 itself, whereas the macropores were generated by the direct removal of PS templates. Due to the large surface-to-volume ratio and regular macroporous structure, 3DOM-ZIF-8 based sensors show good sensitivity and excellent response performance, and can simultaneously detect environmental parameters, including humidity change and harmful gas concentrations. The dispersed ZnO within a hierarchically ordered macroporous-mesoporous-microporous carbon matrix (ZnO@HOMC) was obtained after pyrolysis carbonization of 3DOM ZIF-8 under 350 °C.

3DOM ZIF-8 was subsequently characterized by field-emission scanning electron microscopy (FESEM) and transmission electron microscopy (TEM) in detail. FESEM and TEM images in **Figure 2**a-e show that 3DOM ZIF-8 has a tetrakaidecahedron morphology with an oriented arrangement of ordered macroporous structure (Figures S1, S2, Supporting Information). The 3DOM ZIF-8 possesses a relatively uniform arranged macroporous structure with a pore size of ≈250 nm, which could promote mass transfer (Figure 2b).[29] The FESEM image in Figure 2c indicates that the wall thickness between the macropores is ≈30 nm, which is conducive to the penetration of gas and liquid. The elemental mapping investigation indicates the coexistence of uniformly distributed C, N, Zn, and O elements in the ordered macroporous framework (Figure 2f). The Energy dispersive spectrum (EDS) and the calculated weight percentages and atomic percentages of the 3DOM ZIF-8 further confirms this result (Figure S3, Supporting Information). After pyrolysis under 350 °C, the morphology of ZnO@HOMC does not collapse and the three-dimensional ordered macro-microporous structure remains intact (Figure S4, Supporting Information).

In order to study the crystallographic structure of the 3DOM ZIF-8, X-ray powder diffraction (XRD) measurements was performed (Figure 2g). The powder X-ray diffraction (XRD) analysis confirms that the 3DOM ZIF-8 exhibits the same diffraction pattern as the conventional ZIF-8.[30] There are both 3DOM ZIF-8 and hexagonal ZnO structure detected in the ZnO@HOMC (Figure S5, Supporting Information). This result indicates that the pyrolytic process leads to the formation of ZnO. The N_2 absorption-desorption isotherm plots show typical

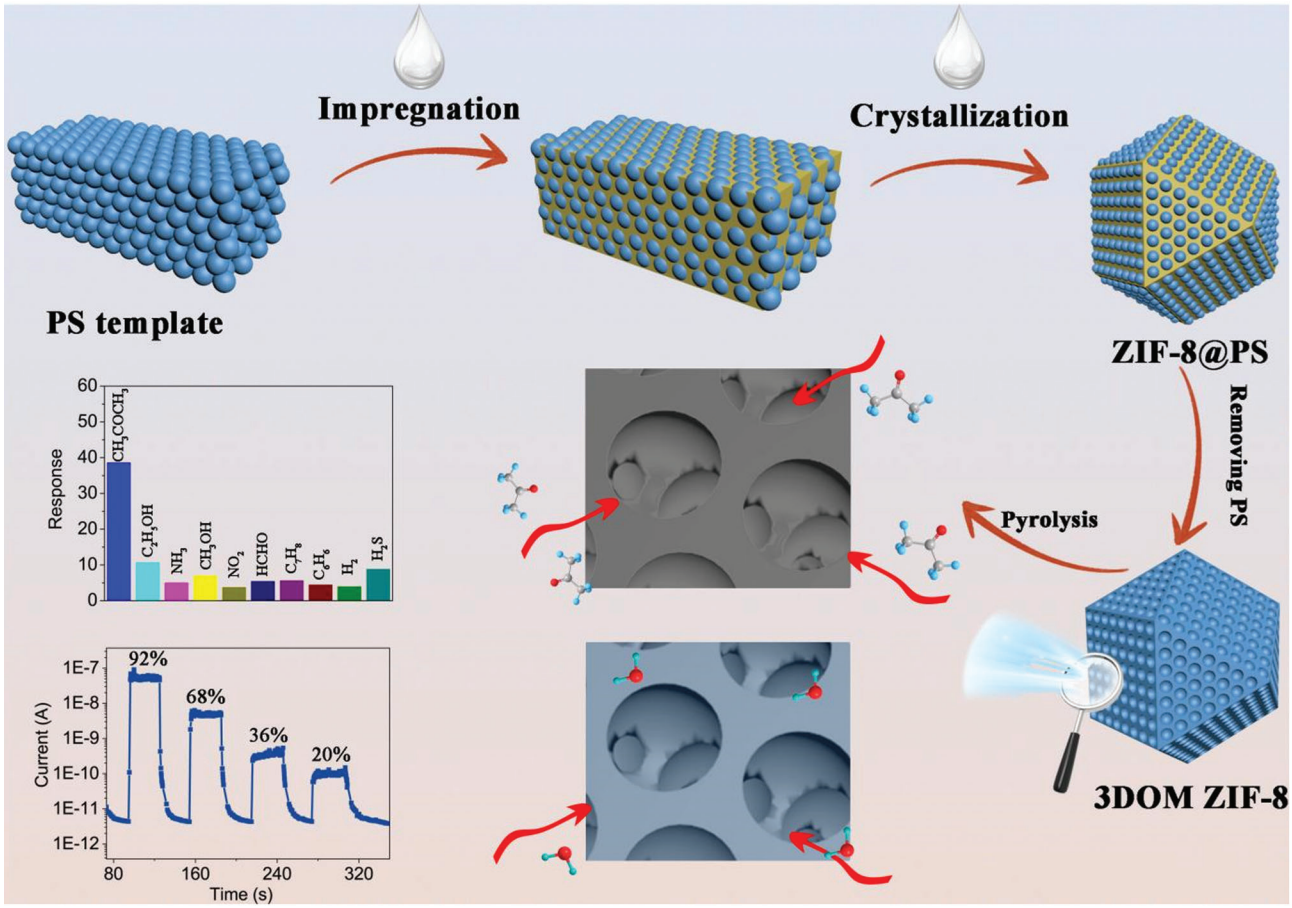

Figure 1. Schematic diagram for in-situ nanocasting synthesis of 3DOM-ZIF-8 and its derivatives (ZnO@HOMC) for the multifunctional sensing application.

type-I isotherm features (Figure 2h), which suggests that the size of pores in 3DOM ZIF-8 is concentrated in the micropore range and the microporous structure was not affected by the 3DOM structure (inset in Figure 2h).[12] The Brunauer-Emmett-Teller (BET) surface area of 3DOM ZIF-8 is calculated to be 558.5 $m^2\ g^{-1}$, which is lower than that of ordinary ZIF-8 (1321.3 $m^2\ g^{-1}$).[25] The decrease of surface area may be related to the reduced content of micropores within 3DOM ZIF-8. X-ray photoelectron spectroscopy (XPS) technique was used to study the chemical states of 3DOM ZIF-8. The existence of C, N, Zn, and O elements can be confirmed in the survey spectrum of 3DOM ZIF-8 (Figure S6, Supporting Information). The spectrum of C 1 s can be divided into two deconvoluted peaks at 283.9 eV and 285.2 eV (Figure 2i), which are assigned to sp^2 hybridized C atoms in aromatic imidazole rings and sp^2 C bonded in the hetero-cycle N≐C–N, respectively.[31] In the Zn 2p spectrum of 3DOM ZIF-8 (Figure 2j), $2p^{3/2}$ state is deconvoluted into two peaks, which are assigned to Zn-N (1020.9 eV) and Zn–O (1021.6 eV) bonds, respectively.[32] The N 1s spectrum of 3DOM ZIF-8 was divided into two functional groups (Figure 2k). The main peaks at ≈399.9 and 398.7 eV were connected with C–N and C≐N in imidazole rings.[33] The O 1s spectrum was divided into two peaks at 532.7 eV and 531.1 eV (Figure 2l), corresponding to O-H in H_2O molecular and hydroxylated Zn.

2.1. Humidity Sensing Performance

The realization of multifunctional detection using one device is of significance to future sensors. The humidity sensing properties of the 3DOM ZIF-8-based device have been measured and the results are shown in **Figure 3**. It is observed that the static resistance of the 3DOM ZIF-8 decreases with the increase of relative humidity (RH) in the air (Figure 3a). The resistance of the 3DOM ZIF-8 in dry air (DA, 6%) is calculated to be $\approx 8.3 \times 10^{12}$ Ω (as deduced from the dark current at 5 V), which is ≈350 times higher than that in 59% RH air (2.43×10^{10} Ω). It is obvious that water vapor in the air has an important influence on the conductivity of the 3DOM ZIF-8. The dynamic current response of the device under different RH circumstances has also been investigated and the results are displayed in Figure 3b. It can be seen that the current changes promptly when the sensor is switched to different RH. The response and recovery time (defined as the time spent to reach 90% of the final equilibrium value) are all less than 1 s (step limitation of the measurement system is 0.23 s). The 3DOM ZIF-8-based sensors in a batch were tested at different RHs, and the impedance signal results are shown in Figure 3c. At humidity range of 21%–99%, the sensors show an impedance change of nearly 4 orders of magnitude, which indicates ultrafast response of the 3DOM ZIF-8 for humidity sensing.

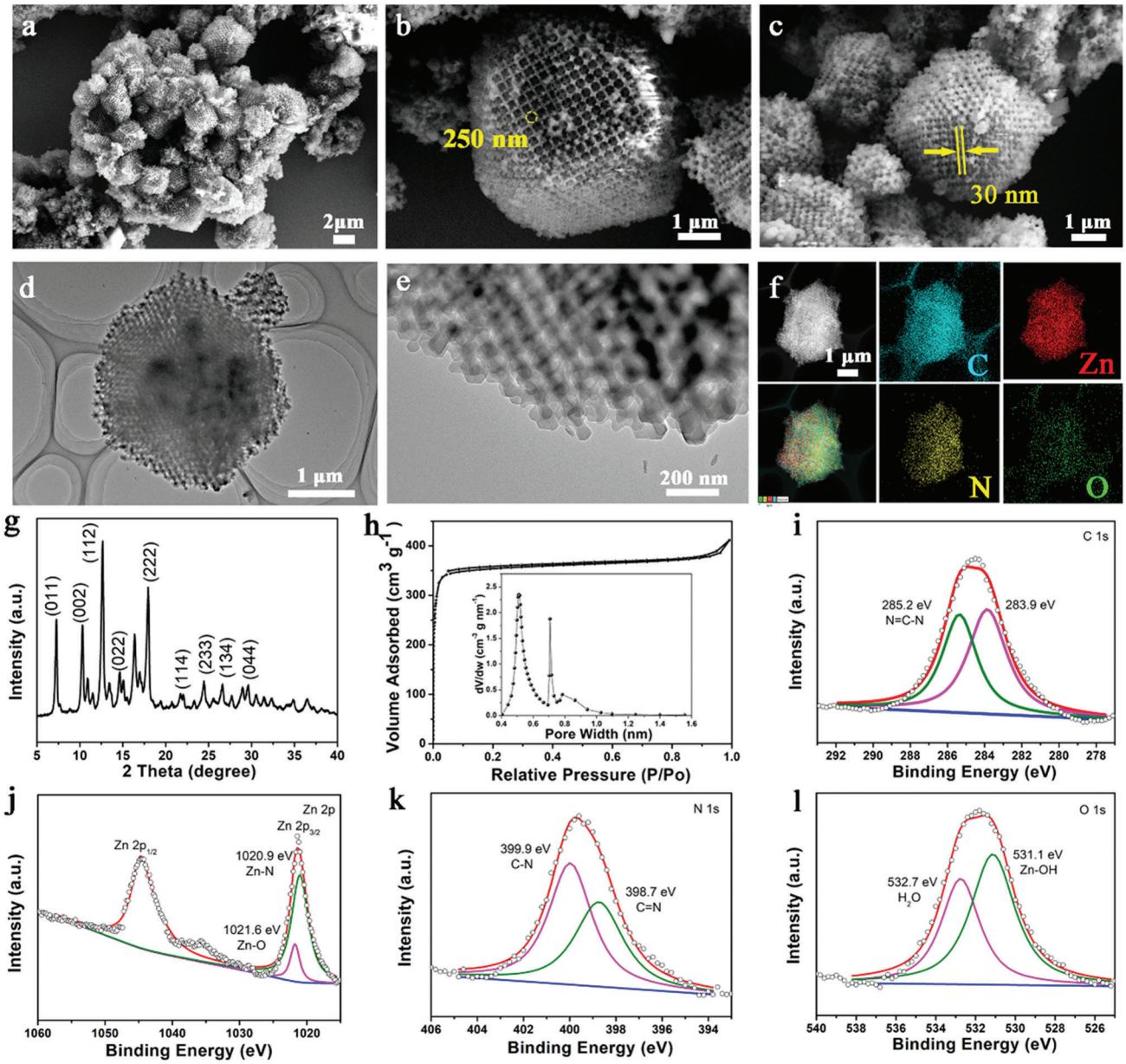

Figure 2. a-c) FESEM images of 3DOM ZIF-8 at different magnifications, d-e) TEM images of 3DOM ZIF-8 at different magnifications. f) TEM image and corresponding EDX elemental mappings of C, N, Zn, and O. g) XRD pattern of 3DOM ZIF-8. h) N_2 adsorption-desorption isotherms of 3DOM ZIF-8. Inset is the corresponding pore size distribution. High-resolution XPS spectra of i) C 1s, j) Zn 2p, k) N 1s, and l) O 1s for 3DOM ZIF-8.

Besides, the responsivity (I_{RH}/I_{DA}) of the 3DOM ZIF-8-based device presents a good linearity with RH in the air (Figure 3d).

In order to verify whether the 3DOM ZIF-8-based humidity sensor has the prospect of application in practical production, the repeatability and stability of the sensor needs to be measured. The continuous response and recovery curve between 21% and 99% RH is shown in Figure 3e, which gives fast response with 4 orders of magnitude, demonstrating perfect repeatability of the sensor. Furthermore, humidity sensor was placed at room temperature for 60 days and measured every 10 days at 21% RH, 33% RH, 57% RH, 76% RH, and 99% RH (Figure 3f). After 60 days, the humidity sensitivity of the sensor almost remained stable within acceptable range. While the response value decreasing to some extent in the environment, which is the result of the combined action of external environment and internal loss. It can be concluded that the prepared humidity sensor based on 3DOM ZIF-8 film has good stability and durability, and shows excellent humidity sensing performances compared to other types of nanomaterials (Table S1, Supporting Information). The as-fabricated humidity sensing device of the 3DOM ZIF-8 is constructed by manually patterning two drops of Ag paste at both ends, and the structure of this sensor is provided in Figure 3g.

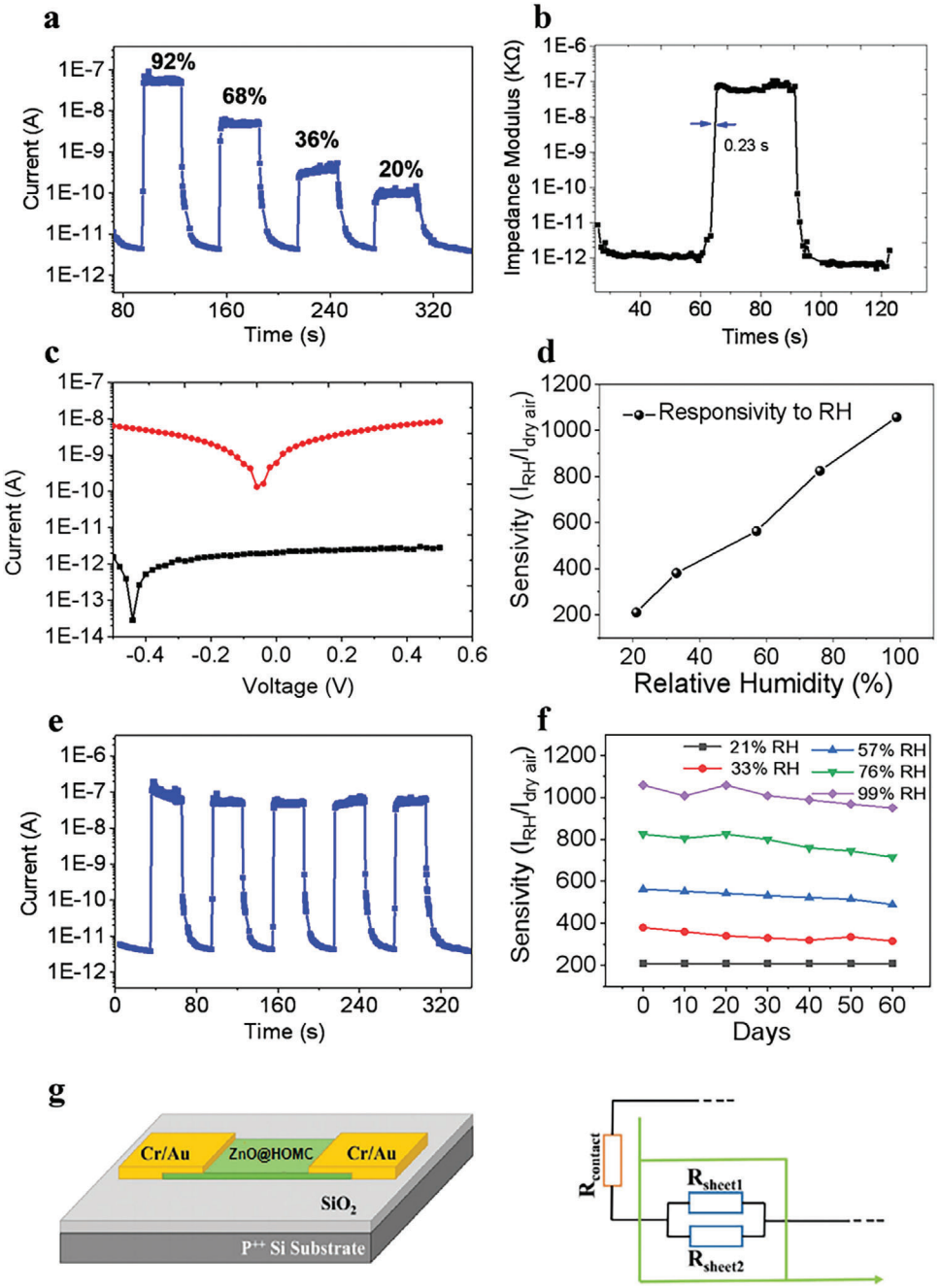

Figure 3. The humidity sensing performances: a) *I–V* curves and b) time response characteristics of the 3DOM ZIF-8-based humidity sensor to dynamic switches between dry air (6%) and different RH (21–99%) at 25 °C and 5 V bias. c) *I–V* characteristics under different RH range at 25 °C. d) Linear dependence of the relation between current response sensitivity and relative humidity at 25 °C. e) Continuous response and recovery curve between 21% and 99% RH for five cycles at 25 °C. f) Long-term stability of the sensor at different ambient humidity at 25 °C. g) The structure of the humidity sensors.

2.2. Gas Sensing Performance

The ZnO@HOMC was used as sensing material to fabricate a semiconductor gas sensor, which shows good sensing performances towards acetone (Figure S7, Supporting Information). First, to determine the optimum working temperature, the sensor was tested to 50 ppm acetone at different working temperatures (200–400 °C), and showed highest sensing response at 350 °C (**Figure 4**a). Then, the sensor was tested to 1, 2, 5, 10, 20, 50, 100, 200, and 500 ppm acetone at 350 °C, and the sensor showed increasing sensitivity from 4.6 to 101(Figure 4b,c). Obviously, the limit of detection (LOD) is <1 ppm. Finally, the sensor was tested to 50 ppm acetone and cycled for six times, the sensitivity was well maintained, indicating good long-term stability (Figure 4d). The

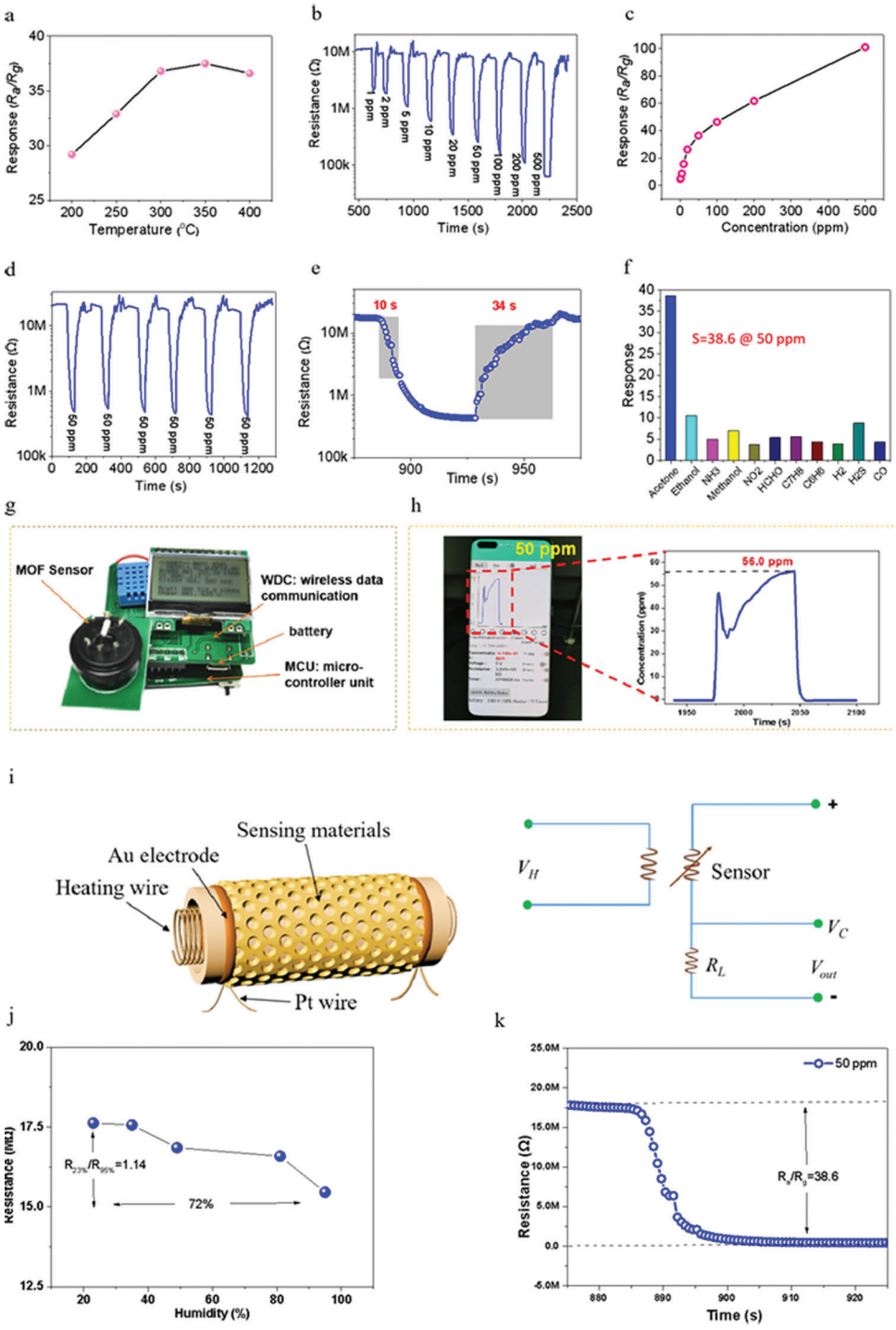

Figure 4. Gas sensing performances of the ZnO@HOMC: a) Responses to 50 ppm acetone at different working temperatures, b) dynamic response-recovery curves at different concentrations (0.5–500 ppm) at 350 °C, c) responses to acetone of different concentration (0.5–500 ppm), d) long-term stability to 50 ppm acetone, e) response-recovery times to 50 ppm acetone, and f) responses to different gases of 50 ppm. g) Optical photos of sensor module wirelessly connected to a smartphone, h) real-time monitoring of acetone concentration on a smartphone (MCU: micro-controller unit, WDC: wireless data communication), i) sketch of the structure of side-heated gas sensor and an electric circuit for gas sensing test, j) resistance of the sensor at different relative humidity (RH), and k) resistance of the sensor when a response to 50 ppm acetone.

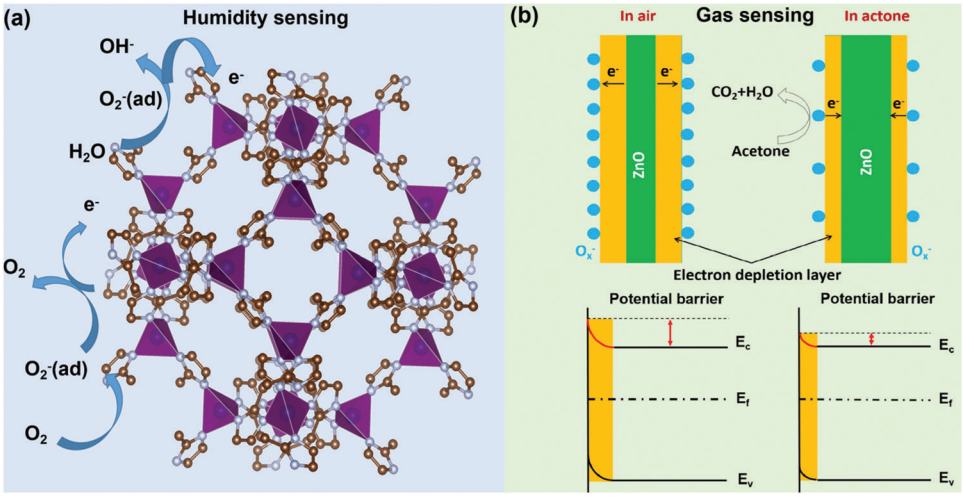

Figure 5. Schematic illustration of the mechanism of a) gas sensing and b) humidity sensing.

gas sensing dynamic was also fast, and the response and recovery time was 10 s and 34 s respectively to 50 ppm acetone (Figure 4e). The sensor also shows high selectivity to acetone, as compared with other nine kinds of interfering gases including ethanol, ammonia, methanol, nitrogen dioxide, formaldehyde, toluene, benzene, hydrogen, and hydrogen sulfide. The sensitivity to acetone (R_{air}/R_{gas} = 38.6@50 ppm) is significantly much higher than other gases, and all the sensitivities of them were <11.0 (Figure 4f). Compared to previously reported acetone sensors,[34–39] the intelligent multifunctional sensor based on ZnO@HOMC shows an obviously outstanding comprehensive performance, including lower detection limit, higher sensitivity, faster response-recovery speed, excellent selectivity, and good long-term stability (Table S2, Supporting Information).

In order to realize real-time monitoring of gas concentrations on mobile devices, a portable sensing module wirelessly connected to a smartphone via Bluetooth communication was fabricated to detect acetone in the atmosphere. The module was composed of a senor based on our 1 wt.% ZnO@HOMC, a battery, a micro-controller unit (MCU), and a wireless data communication (WDC) part (Figure 4g,h).[1] Sketch of the structure of side-heated gas sensor and electric circuit for gas sensing test in Figure 4i. The baseline at different relative humidity were measured, 1% RH change has the same effect on the sensor signal than 0.021 ppm target gas concentration acetone change (Figure 4j and Figure 4k). The integrated sensor module was tested to 10, 20, and 50 ppm acetone respectively, and the sensor output a concentration signal of 11.2, 19.6, and 56.0 ppm respectively, with an error within 12% (Figures S8–S11, Supporting Information). Through the signal conversion systems in the device, the concentration of acetone could be monitored in real time through the App in the smartphone, and the concentration can be displayed directly on the screen. The working principle of the wireless gas sensor module are described in detail in Figure S12, Supporting Information. Therefore, it is expected that the high-performance sensor module highlight the intelligent applications for real-time monitoring concentration of target gases in industrial and agricultural production, human exhalation, and many other fields.

The possible humidity sensing mechanism of the 3DOM ZIF-8-based device is given in **Figure 5**a. For the 3DOM ZIF-8, it is well known that the oxygen molecules can be adsorbed on the surface through reaction $O_2 + e^- \rightarrow O_2^-$ (ad) (1) under low RH in air, which in turn results in an electron depletion layer and a surface barrier that increases resistance.[19] When the 3DOM ZIF-8 is exposed to a high RH environment, the pre-adsorbed oxygen on the surface can be displaced by competitive physisorption or chemisorption of water molecules.[40] On the one hand, the dissociative adsorption of oxygen molecules release electrons to the 3DOM ZIF-8 through reaction: O_2^- (ad) $\rightarrow O_2 + e^-$ (2).[15] On the other hand, the chemisorption of water molecules also provide electrons to 3DOM ZIF-8 via the dissociation of water which can be described in terms of Lewis acid-base reaction: H_2O+O—O+3DOM ZIF-8→OH^-+$HOO^+ + e^-$ (3).[14] Both chemisorption of water molecules and the dissociative adsorption of oxygen molecules processes enhance the concentration of electrons in the 3DOM ZIF-8, leading to the decrease of resistance under a high RH environment.

Due to the adsorption of acetone on the ZnO@HOMC surface, the increase of carrier concentration leads to a drop of the resistance signal. As shown in Figure 5b, when exposed to air, acetone molecules are desorbed from ZnO@HOMC surface and oxygen species are reabsorbed on its surface, forming a wide electron depletion layer (EDL), thus the resistance recovers to the initial value. The acetone molecules desorb immediately from the surface of ZnO@HOMC, and the resistance of the sensor can almost recover to its initial value when the sensor is removed from the acetone atmosphere to clean air, contributing to the good reversibility of the gas sensor. The reaction pathway during the gas sensing process can be described as follows: CH_3COCH_3(ads) + $4O_2^-$(ads) = $3CO_2 + 3H_2O$+$4e^-$ (4).[19] That is, acetone absorbed on the surface of 3DOM ZIF-8 is oxidized into CO_2 and H_2O directly by oxygen species (O_2^-, O^-), meanwhile, electrons flow from acetone to ZnO@HOMC, resulting in a resistance decrease of the sensing layer.[41]

For real application scenarios, a skin humidity analyzer was fabricated based on the principle of biological tissue's electrical characteristics and combined with impedance analysis (Figure

S13, Supporting Information). Based on the skin test module, we can infer and detect the humidity content of human skin through the impedance value. The data collected by the sensors can also be wirelessly transmitted to mobile phones, the user can continuously monitor the skin state. Such a tool will be particularly useful for recording each test data and visualizing the test results, and then evaluate the skin state of dry, normal, or moist at human face and eye socket. At the same time, the humidity sensor can also be used for continuous intelligent monitoring of air environmental humidity in real time and with high precision (Figure S14, Supporting Information). Real-time humidity changes can be monitored during various occasions, ensuring a comfortable environment for the human body.

3. Conclusion

In summary, we designed and constructed a multifunctional sensing system based on 3DOM ZIF-8 and its derivatives. The integrated system can simultaneously monitor the concentration of acetone (LOD < 1 ppm) and humidity (RH 0%–99%), which shows good comprehensive sensing performance including rapid response-recovery speed, high sensitivity, excellent stability, and repeatability. Both the 3DOM ZIF-8 and ZnO@HOMC provide high surface areas with nearly fully exposed active sites, which significantly facilitate the H_2O and CH_3COCH_3 molecules adsorption/desorption, diffusion and transmission for high selectivity under low operating temperature, respectively. Furthermore, the high crystalline framework of the 3DOM ZIF-8 and ZnO@HOMC promote fast transport of charge carriers (i.e., electrons) between surface and bulk for significantly enhanced response-recovery dynamics and sensitivity. Therefore, the 3DOM ZIF-8 is a promising material for fabricating multifunctional sensing device, which can realize real-time tracking of environmental humidity and concentration of volatile organic compounds. Our multifunctional sensing system pave a new way for the next-generation intelligent wearable electronics in breath monitoring and touchless sensing for healthcare applications.

4. Experimental Section

Preparation of 3D ordered PS template: In a typical synthesis, 10 mL of styrene, 0.2 g of PVP, and 100 mL of deionized water were added to a round bottomed flask and bubbled with N_2 for 20 min. Subsequently, the mixture was stirred at 70°C for 10 min in an oil bath to mix well. To initiate the polymerization of styrene, 10 mL of aqueous solution containing 0.2 g of $K_2S_2O_8$ was added into the flask in 20 min. Then the mixture was refluxed at 70 °C with a rotation rate of 800 rpm. After keeping stirring for 24 h, the mixture was cooled down and the monodispersed colloidal polystyrene (PS) spheres were obtained. Finally, a 3D-ordered PS template was obtained by high-speed centrifugation of the PS solution.

Preparation of 3DOM ZIF-8 and ZnO@HOMC: 3DOM ZIF-8 was synthesized according to the reported work.[1] Typically, 8.15 g of $Zn(NO_3)_2{\cdot}6H_2O$ and 6.75 g of 2-methylimidazole were dissolved in 18 g methanol, respectively. Then, the two solutions were mixed quickly, and 20 g of PS template was immersed into the mixed solution for 5 min. The solution was further treated with a vacuum degassing process for 30 min to ensure all PS voids are filled with precursor solution. Then the PS template was dried in a 60 °C oven overnight. The obtained PS template was further immersed into a solution containing methanol and ammonia (1:1 V/V) and keep vacuum for 15 min. Then the mixed solution was held still at ambient temperature for 12 h. The cracked PS template was taken out and dried at 60 °C overnight. Next, the cracked PS template was washed with dimethylformamide and dichloromethane several times and dried at 60 °C overnight to obtain 3DOM ZIF-8. The ZnO@HOMC with dispersed ZnO within a hierarchically ordered macroporous-mesoporous-microporous carbon matrix was obtained after pyrolysis carbonization of 3DOM ZIF-8 under 350 °C.

Gas Sensing Tests: Gas sensing measurements were carried out on a gas sensing system of MA1.0 (XiaoYu Electronics Co. Ltd., China). The side-heated gas sensors were fabricated according to the following procedures. The powder samples (ZnO@HOMC) were mixed and grounded with ethanol to form a paste, which was then coated on an alumina tube attached to a pair of Au electrodes. After drying at 100 °C for 2 h, a Ni-Cr alloy wire was inserted into the tube as a heater. The assembled sensor was then aged at 250 °C for 12 h before measurement. Target gas, such as acetone, was injected onto a heating plate to evaporate and mix with air in the gas chamber. The resistance of a sensor in the air (R_a) and in target gas (R_g) was measured in real-time. The response of the sensor is defined as R_a/R_g. The response or recovery times was defined as the time required for the sensor to reach 90% of the variation in resistance after switching atmosphere.

Humidity Sensing Tests: 3DOM ZIF-8-based humidity sensing device were fabricated by a facile manually operate process. Specifically, 3DOM ZIF-8 suspension is rotated onto the SiO_2/Si substrate, two drops of Ag paste were manually patterned on the 3DOM ZIF-8 thin film to serve as electrodes. For the measurements of the 3DOM ZIF-8-based device as a humidity sensor, I–V curves were obtained by putting the device into the spare space of different saturated salt solutions (LiBr, $MgCl_2$, NaBr, NaCl, and K_2SO_4 which yielded 6%, 34%, 59%, 74%, and 99% RH, respectively, were used to act as humidity source) in airtight closed glass chambers at room temperature. While *I–t* curves were obtained by alternative changing the humidity environment from LiBr to other saturated salt solutions.

Supporting Information

Supporting Information is available from the Wiley Online Library or from the author.

Acknowledgements

J.W. and Y.R. contributed equally to this work. The work was supported by the National Natural Science Foundation of China (No. 12061131009, 92263106, and 12211530438), the Inner Mongolia Talent Fund, Shanghai 2023 "Science and Technology Innovation Action Plan" Star Project (Yangfan Special, 23YF1401700), Youth Talent Introduction Program (JIH2306031Y), and Science and Technology Commission of Shanghai Municipality (No. 21520712600 and 19520744300).

Conflict of Interest

The authors declare no conflict of interest.

Data Availability Statement

The data that support the findings of this study are available in the supplementary material of this article.

Keywords

intelligent devices, metal-organic frameworks, multifunctional sensing, three-dimensional ordered macro-microporous structures

Received: January 10, 2023
Revised: March 25, 2023
Published online: April 28, 2023

[1] M. M. Shulaker, G. Hills, R. S. Park, R. T. Howe, K. Saraswat, H. P. Wong, S. Mitra, *Nature* **2017**, *547*, 74.
[2] X. Zhang, Z. Chen, X. Liu, S. L. Hanna, X. Wang, R. Taheri-Ledari, A. Maleki, P. Li, O. K. Farha, *Chem. Soc. Rev.* **2020**, *49*, 7406.
[3] Y. Liu, Y. Wei, M. Liu, Y. Bai, X. Wang, S. Shang, C. Du, W. Gao, J. Chen, Y. Liu, *Adv. Mater.* **2021**, *33*, 2007741.
[4] H. Li, Z. Qin, X. Yang, X. Chen, Y. Li, K. Shen, *ACS Cent. Sci.* **2022**, *8*, 718.
[5] H. Furukawa, K. E. Cordova, M. O'Keeffe, O. M. Yaghi, *Science* **2013**, *341*, 1230444.
[6] L. E. Kreno, K. Leong, O. K. Farha, M. Allendorf, R. P. Van Duyne, J. T. Hupp, *Chem. Rev.* **2012**, *112*, 1105.
[7] D. Feng, T. Lei, M. R. Lukatskaya, J. Park, Z. Huang, M. Lee, L. Shaw, S. Chen, A. A. Yakovenko, A. Kulkarni, J. Xiao, K. Fredrickson, J. B. Tok, X. Zou, Y. Cui, Z. Bao, *Nat. Energy* **2018**, *3*, 30.
[8] S. Bi, L. Hou, W. Dong, Y. Lu, *ACS Appl. Mater. Interfaces* **2021**, *13*, 2100.
[9] Y. Liu, L. Liu, X. Chen, Y. Liu, Y. Han, Y. Cui, *J. Am. Chem. Soc.* **2021**, *143*, 3509.
[10] Z. Yang, D. Zhang, H. Chen, *Sens. Actuators, B* **2019**, *300*, 127037.
[11] G. Y. Jeong, A. K. Singh, M. G. Kim, K. W. Gyak, U. Ryu, K. M. Choi, D. P. Kim, *Nat. Commun.* **2018**, *9*, 3968.
[12] H. Hong, J. Liu, H. Huang, C. Atangana Etogo, X. Yang, B. Guan, L. Zhang, *J Am Chem Soc* **2019**, *141*, 14764.
[13] K. Shen, L. Zhang, X. D. Chen, L. M. Liu, D. L. Zhang, Y. Han, J. Y. Chen, J. L. Long, R. Luque, Y. W. Li, B. Chen, *Science* **2018**, *359*, 206.
[14] H. Liu, C. Zuo, Z. Li, X. Liu, X. S. Fang, *Adv. Electron. Mater.* **2021**, *7*, 2100706.
[15] J. Dai, H. Zhao, X. Lin, S. Liu, Y. Liu, X. Liu, T. Fei, T. Zhang, *ACS Appl. Mater. Interfaces* **2019**, *11*, 6483.
[16] J. Wang, Y. Ren, H. Liu, Z. Li, X. Liu, Y. Deng, X. S. Fang, *Adv. Mater.* **2022**, *34*, 2104958.
[17] Q. Hua, J. Sun, H. Liu, R. Bao, R. Yu, J. Zhai, C. Pan, Z. L. Wang, *Nat. Commun.* **2018**, *9*, 244.
[18] X. Q. Wang, K. H. Chan, Y. Cheng, T. Ding, T. Li, S. Achavananthadith, S. Ahmet, J. S. Ho, G. W. Ho, *Adv. Mater.* **2020**, *32*, 2000351.
[19] Y. Ren, W. Xie, Y. Li, Y. Cui, C. Zeng, K. Yuan, L. Wu, Y. Deng, *ACS Cent. Sci.* **2022**, *8*, 1196.
[20] S. M. S. Rana, M. A. Zahed, M. T. Rahman, M. Salauddin, S. H. Lee, C. Park, P. Maharjan, T. Bhatta, K. Shrestha, J. Y. Park, *Adv. Funct. Mater.* **2021**, *31*, 2105110.
[21] Y. H. Chen, L. X. Su, M. M. Jiang, X. S. Fang, *J. Mater. Sci. Technol.* **2022**, *105*, 259.
[22] Z. Hu, B. J. Deibert, J. Li, *Chem. Soc. Rev.* **2014**, *43*, 5815.
[23] X. Cao, Y. Xiong, J. Sun, X. Zhu, Q. Sun, Z. L. Wang, *Adv. Funct. Mater.* **2021**, *31*, 2102983.
[24] D. Zhang, Z. Yang, Z. Wu, G. Dong, *Sens. Actuators, B* **2019**, *283*, 42.
[25] P. Li, Z. Zhang, Z. Zhuang, J. Guo, Z. Fang, S. L. Fereja, W. Chen, *Anal. Chem.* **2021**, *93*, 7465.
[26] D. Zhang, H. Chen, P. Li, D. Wang, Z. Yang, *IEEE Sens. J.* **2019**, *19*, 2909.
[27] K. Zhan, Y. Zhu, J. Yan, Y. Chen, *Phys. Lett. A* **2020**, *384*, 126678.
[28] S. Yao, P. Ren, R. Song, Y. Liu, Q. Huang, J. Dong, B. T. O'Connor, Y. Zhu, *Adv. Mater.* **2020**, *32*, 1902343.
[29] W. Li, B. Liu, D. Liu, P. Guo, J. Liu, R. Wang, Y. Guo, X. Tu, H. Pan, D. Sun, F. Fang, R. Wu, *Adv. Mater.* **2022**, *34*, 2109605.
[30] X. Hu, X. Liu, X. Zhang, H. Chai, Y. Huang, *Biosens. Bioelectron.* **2018**, *105*, 65.
[31] D. Tuncel, A. N. Ökte, *Catal. Today* **2019**, *328*, 149.
[32] M. B. Haider, *Nanoscale Res. Lett.* **2017**, *12*, 5.
[33] Y. Liu, Y. Huo, X. Wang, S. Yu, Y. Ai, Z. Chen, P. Zhang, L. Chen, G. Song, N. S. Alharbi, S. O. Rabah, X. Wang, *J. Cleaner Prod.* **2021**, *278*, 123216.
[34] Z. Meng, A. Aykanat, K. A. Mirica, *J. Am. Chem. Soc.* **2019**, *141*, 2046.
[35] A. Aykanat, Z. Meng, R. M. Stolz, C. T. Morrell, K. A. Mirica, *Angew. Chem., Int. Ed.* **2021**, *61*, e202113665.
[36] P. G. Choi, T. Fuchigami, K.-I. Kakimoto, Y. Masuda, *ACS Sens.* **2020**, *5*, 1665.
[37] C. Liu, Y. Gu, C. Liu, S. Liu, X. Li, J. Ma, M. Ding, *ACS Sens.* **2021**, *6*, 429.
[38] Y.-M. Jo, K. Lim, J. W. Yoon, Y. K. Jo, Y. K. Moon, H. W. Jang, J.-H. Lee, *ACS Cent. Sci.* **2021**, *7*, 1176.
[39] Y. Lin, W.-H. Li, Y. Wen, G.-E. Wang, X.-L. Ye, G. Xu, *Angew. Chem., Int. Ed.* **2021**, *60*, 25758.
[40] J. Pang, F. Jiang, M. Wu, C. Liu, K. Su, W. Lu, D. Yuan, M. Hong, *Nat. Commun.* **2015**, *6*, 7575.
[41] X. Yang, Y. Shi, K. Xie, S. Fang, Y. Zhang, Y. Deng, *Angew Chem Int Ed Engl* **2022**, *61*, 202207816.